AERODYNAMIC INTERFERENCE IN FULL HELICOPTER CONFIGURATIONS: VALIDATION USING THE HELINOVI DATABASE

A. Visingardi[1], A. Dummel[2], D. Falchero[3], M. Pidd[4], S.G. Voutsinas[5], J. Yin[6]

[1] Centro Italiano Ricerche Aerospaziali, CIRA
Via Maiorise, 81043 Capua (CE), Italy
e-mail: a.visingardi@cira.it

[2] Eurocopter Deutschland, ECD
81663 München, Germany
e-mail: andreas.dummel@eurocopter.com

[3] Eurocopter France, EC
F13725 Marignane-Cedex, France
e-mail: daniele.falchero@eurocopter.com

[4] QinetiQ
Ively Road, Farnborough, Hampshire,
GU14 0LX, United Kingdom
e-mail: mpidd@qinetiq.com

[5] National Technical University of Athens, NTUA
15780 Athens, Greece
e-mail: spyros@fluid.mech.ntua.gr

[6] Deutsches Zentrum für Luft- und Raumfahrt, DLR
38108 Braunschweig, Germany
e-mail: jianping.yin@dlr.de

Key words: Aerodynamic interference, helicopter, HeliNOVI, numerical simulation, tail rotor noise reduction.

Abstract: The present paper summarizes the results obtained during the validation phase of the aerodynamic computational tools performed in the framework of the European research project HeliNOVI and relative to the interactional phenomena arising on a full helicopter configuration. The activity was carried out by exploiting the experimental database produced during the wind tunnel test campaign of the project for a 40% Mach and dynamically scaled BO105 helicopter model. Seven test cases were performed. A climb, a descent and a level flight were chosen as baseline test cases aiming at highlighting the phenomenological differences among three main helicopter flight conditions. The remaining four were dedicated to the analysis of possible tail rotor (TR) modifications in order to alleviate those interactional aspects responsible for high TR noise emissions. The experimental results indicate a low influence of the main rotor (MR) as source noise in 12° climb and 60m/s level flight whereas a predominance during the descent flight because of MR blade vortex interactions. Conversely, the TR noise represents the main source of noise especially in climb flight whereas is irrelevant during the descent flight. The modification of the TR operational characteristics is effective in reducing the interactional aspects and thus the noise emission. The numerical-experimental comparisons highlight the extreme complexity of the aerodynamic phenomena arising on a helicopter during flight. The numerical computations sometimes provide different predictions. It is a common opinion that they are motivated by the summation of the differences in the methodologies as well as trim procedures applied rather than by a specific reason only.

1 INTRODUCTION

The conventional helicopter is close to the edge of its performance envelope. In the future, emphasis is laid on making it a more efficient and environmentally friendly means of transport. Already today the European manufacturers are producing the quietest helicopters in the world and are the market leaders in civil helicopters. In order to maintain this position a continuous research activity to support the industry is mandatory. This has been the primary objective of a series of research projects of which the European research project HeliNOVI (Helicopter Noise and Vibration) [1] can be considered as the logical continuation.

A particular attention in HeliNOVI was devoted to the aerodynamic and aeroacoustic studies of the tail rotor in order to reach a deeper knowledge of the phenomenology related to it. This was motivated by the fact that in contrast to the main rotor, for which the knowledge and understanding of important aeroacoustic mechanisms have substantially been improved over the last two decades, the knowledge on tail rotor noise generating and radiating mechanisms was still in a very rudimentary state although the conventional tail rotor constituted an important source of helicopter noise in some flight conditions. Especially in steep climb and at high speed level flight condition, the tail rotor represents the dominating source of annoyance caused by a flying-over rotorcraft.

Indeed, preliminary tail rotor noise investigations had indicated that the tail rotor represents an autonomous noise source with radiation characteristics depending on the sense of rotation and in addition constitutes a source of interaction noise caused by its operation in the vortical wake of the main rotor and the main rotor hub. According to the strong perturbation of the tail rotor inflow by the main rotor wake and due to the high rotational speed, the tail rotor radiates noise at high harmonic frequency content, which gives strong contributions to the helicopter noise heard on the ground and which is very difficult to predict.

The project was structured in four main work packages: WP1 - Tail Rotor Noise Reduction; WP2 - Helicopter Vibration Reduction; WP3 - Wind Tunnel Tests & Synthesis; WP4 - Management, through which three main deliverables were obtained:

- the production of the first European database for high resolution airloads on rotor blades and fuselage, and for the radiated noise;
- validated prediction tools for tail rotor noise including main/tail rotor interactions suitable for future aircraft design purposes and for retrofit purposes;
- theoretical and experimental demonstration/validation of tail rotor noise and vibration reduction potentials.

The present paper illustrates some of the main results obtained during the phase of the final validation of the aerodynamic computer codes that was achieved by performing code-to-code and code-to-test comparisons by exploiting the experimental database produced during the wind tunnel test campaign of the project for a BO105 helicopter model.

Three research centres: CIRA (I), DLR (D), and QinetiQ (UK); the EUROCOPTER industry; and the NTUA university (GR) participated in this activity [2]. In particular, the experimental dataset was post-processed and provided by DLR to the partners. The detailed information of this activity were illustrated in [3], [4], [5].

The main geometrical and instrumentation characteristics of the BO105 model are illustrated in Section 2 whereas Section 3 provides a description of the test cases performed by the partners for the final validation of the aerodynamic prediction tools. The methodologies applied and the trim procedures followed are briefly described in Section 4. The analysis of the results is provided in detail in Section 5. The main conclusions are drawn in Section 6.

2 THE BO105 WIND TUNNEL MODEL

The wind tunnel model was a 40% dynamically and Mach-scaled BO105 helicopter, Figure 1, consisting of main rotor (MR) blades and a geometrically scaled fuselage including a teetering tail rotor (TR) system [6]. The backbone of the model was the MWM (Modular Wind tunnel Model, [7]) containing in a shell core components like gearbox, rotor shaft and drive train system for the MR. The wind tunnel test campaign was performed in the 8m X 6m open jet test section of the DNW Large-Low speed Facility (LLF).

2.1 Model characteristics

The MR is a geometrically and dynamically scaled model of the four-bladed hingeless BO105 MR with a NACA23012 airfoil whose trailing edge was modified to form a 5 mm long tab in order to match the geometry of the full scale rotor. The blades have a linear twist of -8° and a rectangular planform leading to a solidity of 0.077. The TR is a geometrically scaled model of the two-bladed BO105 see-saw TR. The blades have no twist and a standard square tip. Two sets of TR blades were used: S102 airfoil; NACA0012 airfoil. The rotational speed ratio between the TR and the MR was set to 5:1 for the HeliNOVI test campaign. The fuselage is only geometrically similar to the BO105 rotorcraft since the design and manufacture of a dynamically scaled helicopter fuselage is beyond the conventional technology for helicopter wind tunnel models.

Figure 1: The BO 105 wind tunnel model

The MR and TR main characteristics of the model are given in Table 1 below illustrated.

Property	symbol	main rotor	tail rotor
no. of blades	N_b	4	2
rotor type		hingeless	teetering
radius	R	2m	0.383m
radius scale factor	S	2.456	2.48
chord	c	0.121m	0.074m
root cutout	r_a	0.44m	0.16m
solidity	σ	0.077	0.123
precone	β_p	2.5^o	0^o
pretwist	Θ_t	$-8^o/R$	$0^o/R$
pitch-flap coupling	Δ_3	0^o	45^o
reference tip Mach	M_{tip}	0.64	0.65
lock number	γ	8	4.2
shaft tilt forward	$\epsilon_t,\ \epsilon_x$	3^o	4.2^o
shaft tilt upward	ϵ_z	90^o	3^o
motor axis upward	ϵ	0^o	50^o
airfoil		NACA23012mod	S102E, NACA 0012
drag area	A_{TR}	-	$0.026m^2$
drag coefficient	$C_{w,TR}$	-	0.8

Table 1: MR and TR main characteristics

2.2 Rotors and Fuselage Instrumentations

A total of 118 dynamic pressure sensors were used to fully instrument the model. 51 sensors were placed on MR, 36 sensors on TR and 31 sensors on the fuselage, tail boom and stabilizers (vertical and horizontal).

Two blades of the MR were instrumented with respectively 25 and 26 Kulite pressure transducers. The first blade was mainly instrumented at the radial station at 87% whereas the sensors on the second blade were distributed on several radial stations so as to have in particular a fully instrumented station at 87% and an opportunity to detect any differences between the blades at stations 87% and 97%.

Two sets of TR blades were used, each of them with one blade instrumented. The S102 blade was equipped with 36 sensors, and the NACA0012 blade with 20 sensors. The NACA blade was employed to study the effects of the different TR sense of rotation. On the S102 blade, stations at r/R=0.80 and 0.97 were densely instrumented and the pressure at the leading edge was provided at 4 more radial stations. The NACA0012 blade was densely instrumented only at the 97% station with indication of the pressure at the leading edge provided at three more stations.

2.3 Stereo PIV measurement set-up

A common vertical support with three traverses was employed to carry the two lasers and the camera systems necessary for the stereo PIV measurements. The laser beams were vertically directed into the flow field and aligned on the same plane. One measurement plane was located on the suction side of the tail rotor 64mm away from the disc and the second plane was located on the blowing side 52mm away from the disc, as shown in Figure 2. The PIV trigger was synchronized to the MR azimuth from 0° to 150° with increments of 30°. Thus, the MR tip vortex flight path through the TR disc was covered. Five positions of the observation area, with some overlap, were selected to cover the entire TR area, except where the horizontal stabilizer and its end plates prohibited measurements. The observation area covered 378mm horizontally (almost the TR radius of 383mm) and 339mm vertically.

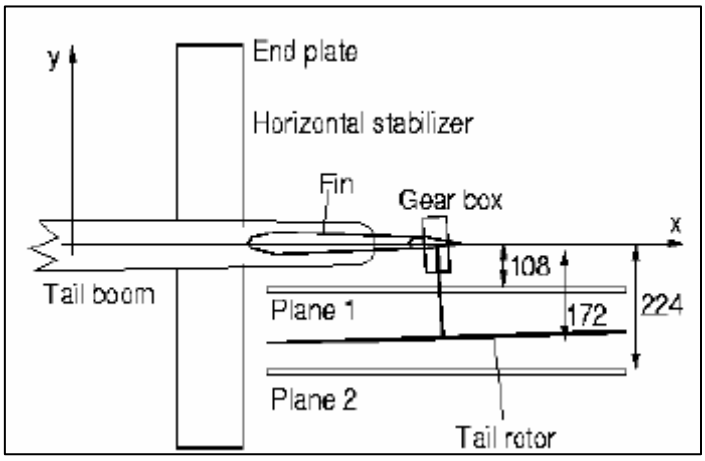

Figure 2: PIV measurement planes on both sides of TR – top view

3 TEST CASES FOR THE FINAL VALIDATION OF THE AERODYNAMIC PREDICTION CODES

The final validation of the aerodynamic prediction codes was performed by making the numerical/experimental comparisons on the following seven test cases:

1. **ID01:** 12º climb at 33m/s equipped with a S102 TR blade airfoil section;
2. **ID02:** level flight at 60m/s equipped with a S102 TR blade airfoil section;
3. **ID05:** 6º descent flight at 33m/s equipped with a S102 TR blade airfoil section;
4. **ID10:** level flight at 60m/s equipped with a S102 TR blade airfoil section and 10% reduced blade tip speed;
5. **ID13.1:** level flight at 60m/s equipped with a S102 TR blade airfoil section and different tail rotor vertical position;
6. **ID13.2:** level flight at 60m/s equipped with a NACA0012 TR blade airfoil section;
7. **ID13.4:** level flight at 60m/s equipped with a NACA0012 TR blade airfoil section and reversed sense of rotation (Advancing side up).

Each of the abovementioned test cases was selected in order to check the prediction codes capabilities to evaluate the aerodynamic and aeroacoustic characteristics of the configuration in different flight conditions and with different TR operational characteristics. The first three cases are baseline tests: ID01 was selected in order to check the codes without expecting complications due to MR BVI; ID02 is a moderate-speed test case where some compressibility effects can be expected at the tip region; ID05 is a descent flight where MR BVI is expected to play an important role. The remaining four test cases are all variants of test case ID02 each of them with a modification of one tail rotor operational characteristic mainly aimed at evaluating its effect on the TR noise emission reduction.

Each partner chose a subset of these test cases. Table 2 summarizes their distribution among the partners:

Test Case	P1	P2	P3	P4	P5	P6
ID01		X	X	X		
ID02		X	X	X	X	X
ID05	X			X		X
ID10		X	X	X		
ID13.1					X	X
ID13.2	X			X	X	X
ID13.4	X			X	X	X

Table 2: Test Case distribution among the partners

4 METHODOLOGIES & TRIM PROCEDURES APPLIED

The final validation was performed by the partners by applying the methodologies and the trim procedures shortly summarized in the following subsections:

4.1 Methodologies

P1 partner applied a chain of codes. It benefited from the experience with comprehensive codes thanks to which all the calculations made are aeroelastic. In particular, with reference to BVI, a special 2D model was developed which deals, in a fine space and time scale, with the interaction of vortex structures with the blades. Compressibility was taken into account by using the Prandtl-Glauert compressibility correction formula. The fuselage was not modelled;

P2 partner applied the commercial CAMRAD II comprehensive rotorcraft code which is based on the blade element theory. All calculations were performed with elastic blades and in incompressible mode. A plug-in of another comprehensive code - CHARM – further enhanced the aerodynamic ability by offering a constant vorticity contour free-wake model as well as a panel method, that allowed the aerodynamic modelling of the fuselage for all the test cases;

P3 partner applied an incompressible, unsteady panel code, which is based on the direct potential representation, to model the whole BO105 configuration under the hypothesis of rigid body motion. All the computations were performed in incompressible mode. Fully compressible computations were additionally performed for two selected test cases: ID02 and ID10 for which the "transpiration angle" weak coupling approach was applied between the panel code and the unsteady full potential HELIFPX code;

P4 partner applied a 3D free-wake incompressible, unsteady panel code which, differently from partner P3 code, is a velocity-based, indirect potential formulation – a combination of source and dipole distribution is used on the solid surfaces and dipole panels in the wake. All the computations were performed in incompressible mode, the fuselage was not modelled and the rotor blades were considered as rigid;

P5 partner applied a chain of codes to the problem. Initially a wind-tunnel trim procedure was applied for the non-interacting main and tail rotor. A subsequent time-domain calculation was performed, using the pre-calculated cyclics and collectives, for the interacting main and tail rotor configuration. Both these calculations included elastic effects using codes from the CRFM suite. A final aerodynamic analysis was performed using the HELIFPXQ full-potential code incorporating aeroelastic and wake interaction effects through an imposed transpiration velocity. The fuselage was not modelled;

P6 partner applied an integrated model capable of performing simultaneously aerodynamic and aeroelastic calculations. The aerodynamic part is based on an unsteady vortex particle model coupled with a low-order panel method. The computations were corrected for compressibility effects by using the Prandtl-Glauert formula. Main and tail rotor blades were modelled as flexible bodies whereas the fuselage was assumed rigid. Fully compressible computations were additionally performed for the ID02 test case by locally applying a 2D Euler code on a section by section basis.

4.2 Trim procedures

The procedures applied by each partner are briefly described in the following:

P1 partner performed both a force and a control angle trim procedures for the main rotor calculations by the application of the aeromechanic HOST code. Only a force trim procedure was instead used for the TR;

P2 partner evaluated the trim control angles by the application of a force trim procedure to match the experimental MR thrust, pitching and rolling moments and the TR thrust;

P3 partner applied the experimentally evaluated trim control angles apart from the collective pitch values that was modified in order to obtain an average value of both MR and TR thrust coefficients equal to the experimental ones;

P4 partner evaluated the trim control angles by the application of a force trim procedure to match the experimental MR thrust, pitching and rolling moments. The trim procedure was started with the isolated MR. After MR thrust, pitching and rolling moments matching with experiment value was reached, the TR was then added into the computation and the TR trim started by assuming that the effect of TR would not change the MR trim value;

P5 partner derived an initial trim to the MR thrust and pitching and rolling moments. The TR was trimmed to thrust alone. The collectives and cyclic resulting from this initial non-interacting calculation were then applied to the full simulation;

P6 partner evaluated the trim control angles by the application of a force trim procedure to match the experimental MR thrust and moments and TR thrust.

Table 3 summarizes the configuration modelling parameters and the trim procedures applied by the partners for the final validation computations.

Partner	Compressibility	Blade Flexibility	Fuselage Modelling	Trim Procedure
P1	P-G	MR only	NO	Force & Control Angle Trim
P2	Look-up tables	YES	YES	Force Trim
P3	NO	NO	YES	Collective pitch modification
P4	NO	NO	NO	Force Trim
P5	YES	YES	NO	Force Trim
P6	P-G	YES	YES	Force Trim

Table 3: Configuration modelling parameters & Trim procedures

5 ANALYSIS OF THE RESULTS

The numerical/experimental aerodynamic comparisons were performed at different scales:

- the rotor scale, in which the global loads on the main and tail rotors were recorded. In this scale two aspects were analysed and checked: (a) the quality of convergence in time, and (b) the comparability between the different sets of predictions;
- the blade scale, in which the time evolution of the normal force at specific radial stations of both rotors were recorded. In this scale the main aspect checked concerns the wake-induced effects on both the main and tail rotor. This includes BVI encounters and less local effects such as the variation of the normal load over the upstream part of the MR disc. The interaction between the two rotors was also checked even though the time scale used by the prediction codes was rather coarse for the TR since the smallest time step used led to a TR azimuthal step of 5º;
- the sectional or local scale, in which the instantaneous pressure distributions at specific blade sections and time instants were recorded. The pressure distributions provided a means for cross checking the results in the blade scale. In addition, they made the analysis of compressibility effects possible for those cases where the compressible flow equations were solved;
- the flow field scale, in which the three components of the velocities induced by the configuration during the flight were recorded in order to detect the details of the vortical structure of the wake system.

For all the flight conditions the BO105 model was trimmed at a similar vertical force, measured with respect to its centre of gravity, leading also to similar main rotor thrust coefficients, Table 4. The exception of ID10 was the consequence of the different non-dimensionalization resulting from the lower MR and TR angular velocities.

Test Point	Fz_CG	CT Main Rotor	CT Tail Rotor
ID01	-3818.40	0.00538	0.00652
ID02	-3695.20	0.00521	0.00418
ID05	-3750.10	0.00511	0.00159
ID10	-3711.20	0.00648	0.00540
ID13.1	-3690.30	0.00544	0.00443
ID13.2	-3684.70	0.00528	0.00402
ID13.4	-3686.40	0.00523	0.00443

Table 4: Trim vertical force (Fz) and MR/TR thrust coefficients (CT)

The results illustrated in this section are an excerpt from the huge numerical-experimental database produced during the project, aiming at illustrating the phenomenological differences among the selected test cases and highlighting the abilities, as well as the limitations, of the methodologies and trim procedures applied.

5.1 Main rotor sectional normal loads

The MR sectional normal loads for the three baseline test cases are illustrated in Figure 3. The experimental results for the climb flight ID01 indicate a low-frequency behaviour throughout the revolution with a light, localised change in the CN time evolution around 130° that is due to the non-negligible influence of the tip vortex trailed by the preceding blade on the main blade because of the relatively low flight velocity. Also, a drop in the load occurs around 240°. During the moderate-speed level flight ID02 a sort of CN "bucket" can be observed in the experiment that extends from approximately 100° to 150° with the minimum located around 130°. This phenomenon is likely to be determined by the co-existence of important compressibility, aeroelastic and interactional effects; nevertheless, the details of it are neither very clear nor definite conclusions can be inferred from the analysis of only one blade sec-

tional load. A sudden drop in CN is present around 270° due to the interaction of the main blade with the tip vortex trailed by the preceding blade. Finally, the high frequency fluctuations in the experimental sectional load during the ID05 descent flight clearly indicate the presence of strong BVI phenomena in the downstream region of the MR disc which make the MR the dominating factor of the total noise radiation during this flight condition.

The numerical predictions obtained for the ID01 test case show a mean CN value overestimated in the results of P2 whereas a sufficient agreement up to 270° can be observed in P4 results. The localised CN variations around 130° in P3 results seem to reproduce the physical blade-vortex interaction; furthermore, the particular trim procedure used in the P3 predictions is a plausible explanation of the under-estimation in the retreating side of the rotor disc. Finally, all the predictions delay the experimental CN relative minimum located around 270°. All the predictions for the ID02 test case are unable to correctly locate the CN bucket, all showing an anticipated prediction of it. The sudden drop at 270° is correctly predicted despite differences in value and location of the CN maximum can be observed. In particular, the results of P5 show a general phase shift in anticipation. Despite the phenomenological complexity of the descent flight all the predictions show a satisfactory ability to model the CN fluctuations in the downstream region of the rotor disc whereas remarkable differences can be observed in the rotor disc upstream region. The results obtained by P6 show a good correlation with measurements which is attributed to the low speed, so that compressibility effects are not important, and to the account of the aeroelastic coupling.

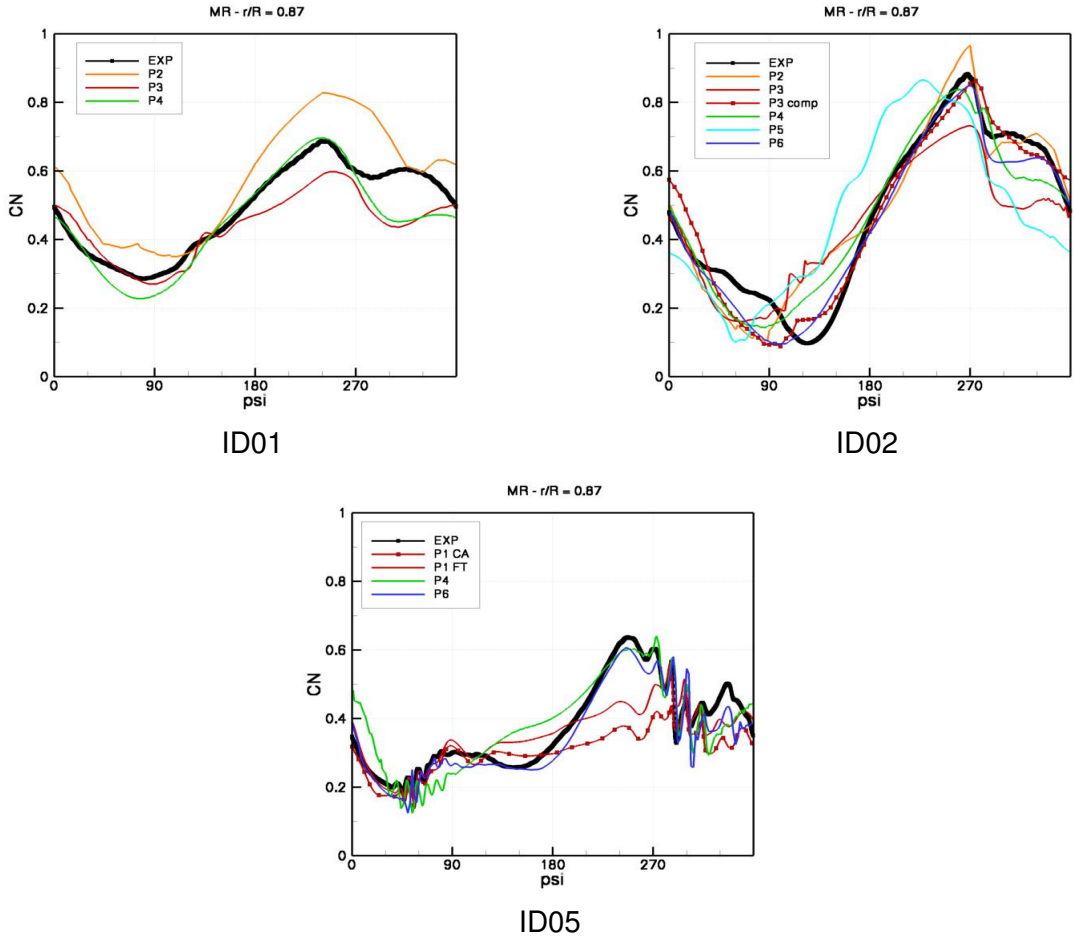

Figure 3: MR Sectional normal loads for the baseline test cases

The modifications of the TR operational characteristics for the moderate-speed level flight determined mild qualitative changes in the experimental MR sectional loads: the tip speed reduction, ID10, cancels the CN bucket on the blade advancing side and reduces significantly the CN drop at 270°. Conversely, a more defined formation of the CN bucket can be observed as the TR sense of rotation is reversed, ID13.4. Instead, the higher vertical position of the TR disc determines a slightly higher CN maximum around 270°. The numerical predictions were slightly affected by the TR modifications. Only for ID10 the results obtained by P3 are generally over-estimating the experimental load whereas the CN bucket predicted by P2 is, contrary to the experiment, more pronounced with respect to the baseline condition.

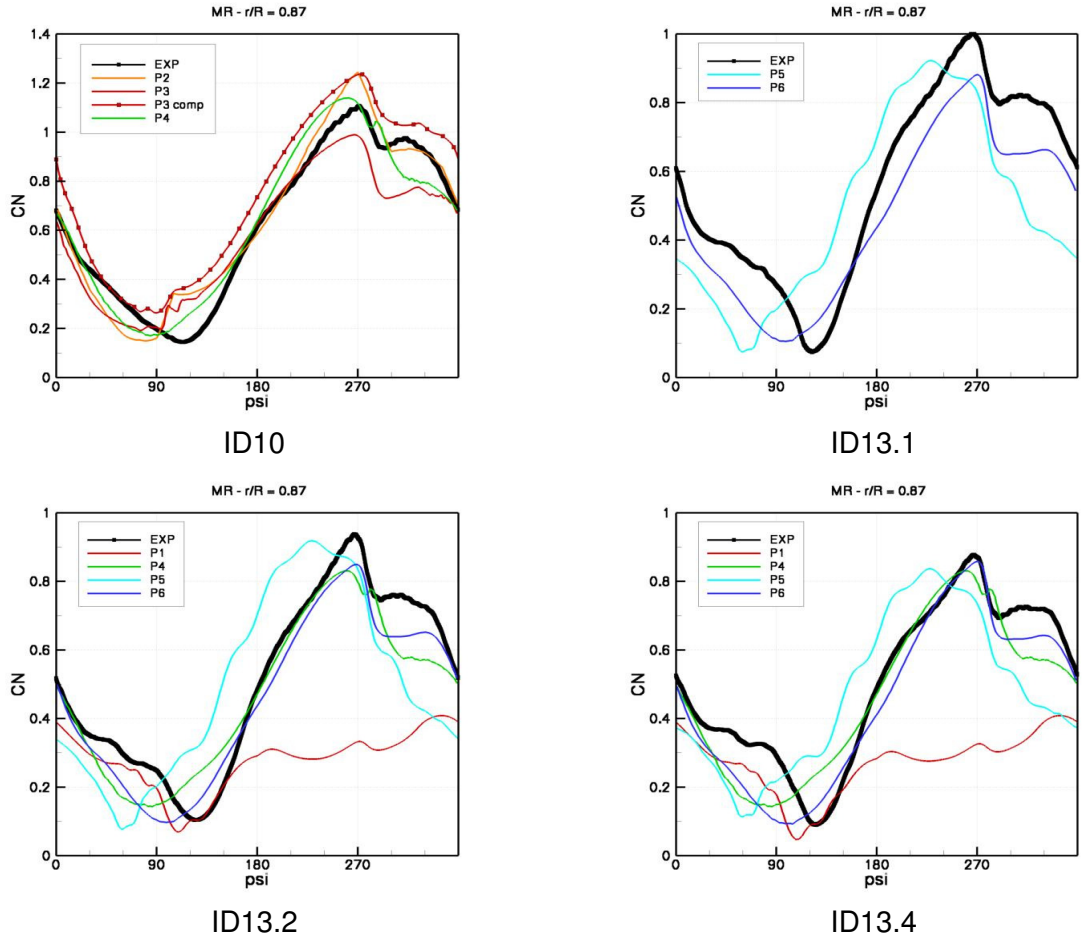

Figure 4: MR Sectional normal loads for the baseline test cases

5.2 Tail rotor sectional normal loads

The TR sectional normal loads at the radial section r/R= 0.80 for the three baseline test cases are illustrated in Figure 5. Since the TR is five times faster than the MR the representations correspond to one complete MR revolution. Within each TR revolution the experimental results show a sequence of CN maxima and minima approximately located in the same azimuthal positions regardless of the flight condition. The main differences are observable in terms of CN mean value, resulting from the flight speed and the trim condition of the whole configuration, and of the frequency content and fluctuation amplitudes which arise basically for the following three reasons: 1) TR blade passage in the vicinity of the vertical fin; 2) TR blade interaction with the MR blade tip vortices; 3) TR blade interaction with the TR blade tip vortices.

The difference in the relative importance of these reasons can have a significant impact on the TR noise emission. Indeed, during the climb flight, ID01, the MR wake interacts more directly with the TR. The resulting frequency content and high amplitude fluctuations in the load make the TR an important source of radiation noise for this flight condition. During the level flight at moderate speed, ID02, the amplitude fluctuations are less pronounced but the frequency content and the flight speed play an important role in the TR noise emission. In the case of the descent flight, ID05, the MR wake does not interact with the TR. As observed in the figure, the normal load shows a low amplitude and frequency content and a reduced mean CN value thus making the TR almost irrelevant as far as the noise emission is concerned.

The numerical analysis of ID01 indicates the presence of slight phase shifts in the predictions of P3 and P4, an over-estimation of the peak located at each 270° in the predictions of P2 and P3, and a considerable under-prediction by P3 in the downstream region of the TR disc. Differences with the experiment in terms of frequency content can be observed in the P3 and P4 predictions whereas P2 show a satisfactory behaviour. A good correlation with the experiment is shown for ID02 in the P3 and P6 predictions. A slight phase shift, together with an over-estimation in the maximum CN peaks, can be observed in P4 computations whereas the P5 results show the inability to detect the details of the TR interactional process. The numerical investigation of the descent flight, ID05, shows a good capability of all the predictions to detect the whole interactional process in terms of amplitude and CN mean value but disagree with the experimental time evolution.

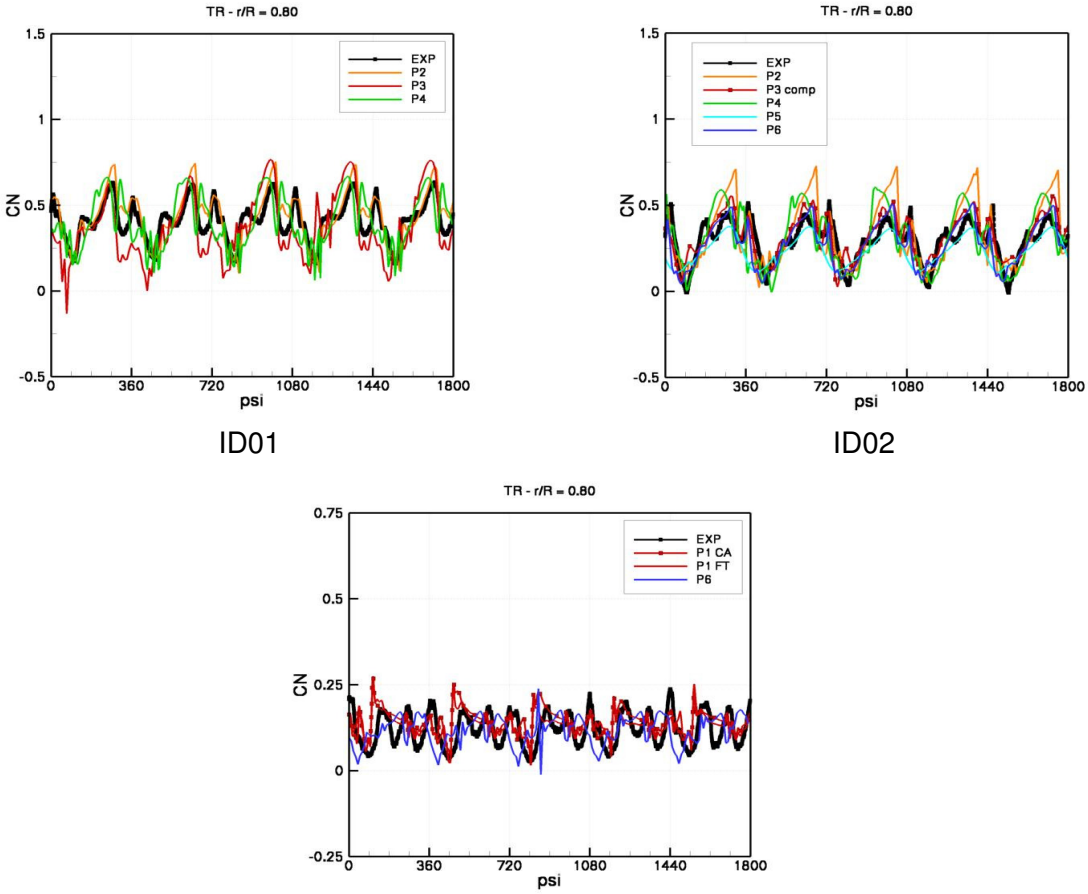

Figure 5: TR Sectional normal loads for the baseline test cases at r/R = 0.80

The TR sectional normal loads at the radial section r/R= 0.80 for the TR-modified test cases are illustrated in Figure 6. The experimental results at this radial section were available only for the ID10 and ID13.1 test cases. The reduction of the blade tip speed , ID10, determines an increase in the load amplitude but a reduction of the frequency content in the load time evolution. These two aspects, together with the lower blade speed results in a less noisy condition. The translation of the TR to a higher vertical position, ID13.1, reduces the TR interaction with the MR wake system thus determining a significant reduction of the frequency content of the load time evolution and creating a good premise for a quieter configuration.

The P3 simulation of ID10 test condition shows a sort of phase shift with a higher amplitude of the time evolution; the maximum CN is over-estimated The P4 predictions are basically aligned with the P3 ones with only a better evaluation of the CN minimum peaks. In comparison with the two previously discussed numerical computations the P2 predictions slightly postpone the maximum CN peak location but the value is similar. The prediction is however satisfactory. The P6 evaluation of the ID13.1 test case is in a satisfactory agreement with the experiment but the CN minimum location is slightly anticipated. P5 predictions differ substantially from the experiment mainly in terms of phase and frequency content.

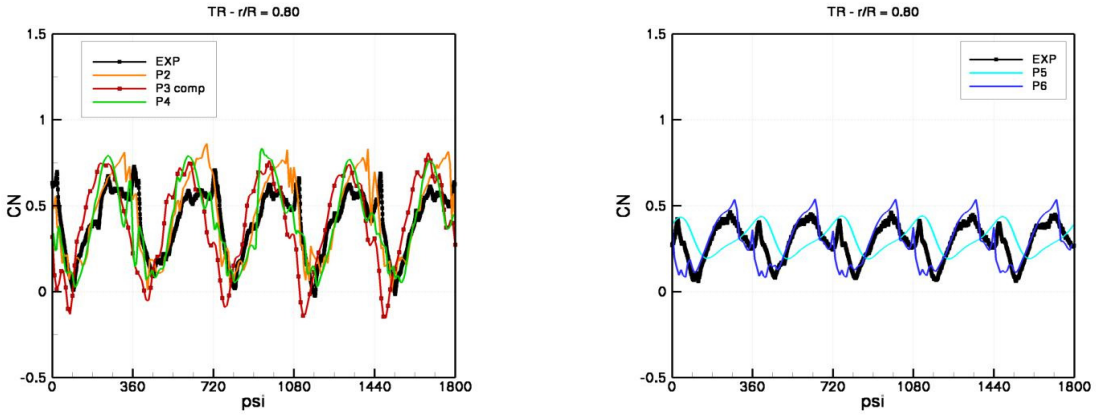

ID10 ID13.1

Figure 6: TR Sectional loads for the TR-modified test cases at r/R = 0.80

5.3 Main and tail rotor pressure time histories

Sample figures of the main and tail rotor pressure time histories are provided in the present subsection. Since it is well known that the leading edge of a blade plays the role of predominant source of noise radiation, the pictures illustrate the time histories evaluated at the chordwise section x/c = 0.03.

Figure 7 illustrates a comparison, both numerical and experimental, between the pressure time evolutions for the MR during the moderate-speed level flight ID02 and the descent flight ID05. In the first case the experimental result shows a regular behaviour with a sudden change in slope at 270° exactly reproducing what can be observed in terms of normal load (Figure 3). All the numerical computations show the ability to correctly locate the sudden change of slope whereas some differences in terms of Cp mean value or Cp maximum expansion evaluation can be observed. The compressible computations of P3 and P6 show, in particular, a global satisfactory agreement with the experiment. The high-frequency pressure fluctuations in the ID05 test case highlight the role of the MR as the main source of noise radiation in descent flight. P1 and P6 numerical computations are able to correctly model the phenomenology. Some discrepancies with the experiment can be observed in the P4 results.

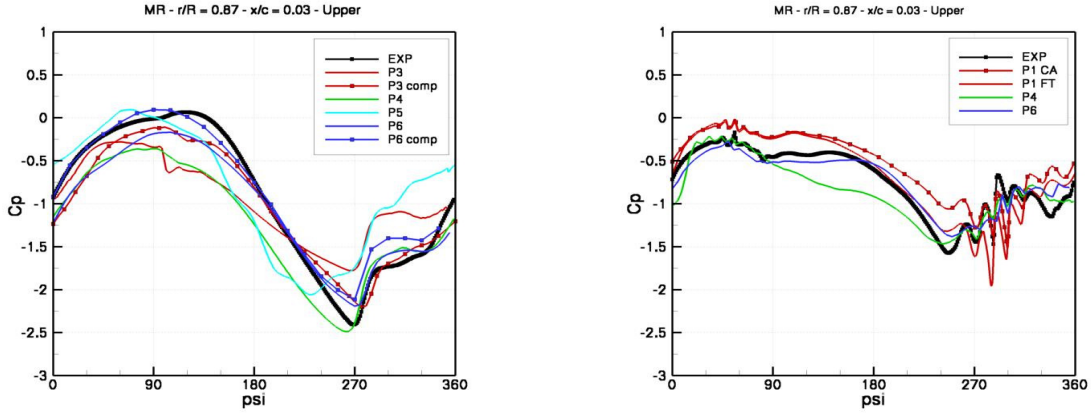

ID02 ID05

Figure 7: MR pressure coefficient time histories at chordwise station x/c = 0.03 and radial station r/R = 0.87

Figure 8. illustrates the between predicted and measured pressure time evolutions for the TR for the three baseline test cases and the TR-modified test case ID10. The high amplitude, peaky experimental behaviour of ID01 indicates the strong influence of the TR to the noise emission in this test condition. The P3 numerical results are in a general qualitative good agreement with the experiment thus indicating that the main phenomenological aspects resulting from the TR blade interaction with MR blade tip vortices and the presence of the fuselage are correctly modelled. Some quantitative differences are however present in terms of phase shift and intensity of the Cp peaks. The P4 results indicate a smoother time evolution which could arise from the absence of the fuselage in the computation. The moderate-speed level flight ID02 exhibits a smoother fluctuation of the experimental pressure thus indicating a reduced contribution to the noise emission. Not all the numerical computations are able to correctly predict the details of the time evolution. A sort of slight phase shift, in anticipation, is generally observed. In some cases the mean value disagrees with the experimental one. The descent flight ID05 shows a small amplitude of the Cp time evolution. The numerical predictions, despite a different qualitative evaluation of the time evolution, are however able to correctly evaluate both the amplitude and the mean value of the pressure coefficient. Finally, the TR-modified ID10 test case shows a higher amplitude in the time evolution in comparison with the respective baseline test case ID02 but the frequency content is slightly reduced. This would imply an improvement in the TR noise reduction. The two sets of the numerical predictions both show a phase shift and are not fully able to evaluate the experimental sudden changes in slope (e.g. at each 360°). The main reason is the size of the time step, 5° in the P4 and 10° in the P3 simulations, which are insufficient to capture these details in the pressure time evolution.

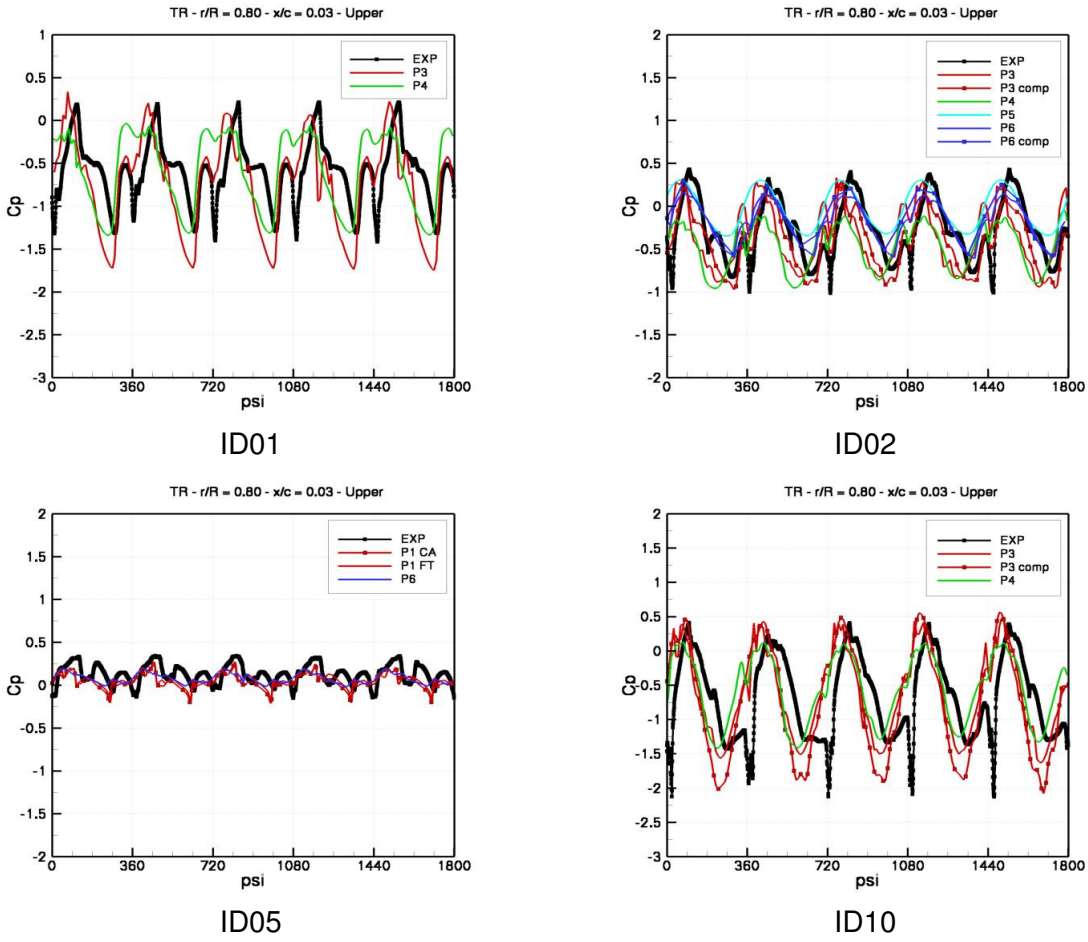

Figure 8: TR pressure coefficient time histories at chordwise station x/c = 0.03 and radial station r/R = 0.80

5.4 Main and tail rotor chordwise pressure distributions

Finally, a few examples of the experimental and numerically evaluated chordwise pressure coefficients are provided in this subsection in order to highlight some chordwise phenomenological details and some critical points in the numerical simulations.

Figure 9 shows the pressure coefficients at two different azimuthal steps for the ID02 test case. The presence of compressibility effects for this moderate-speed flight condition is clearly indicated in the results at 90°. Only the fully compressible P5 and P6 predictions are able to detect the formation of a shock wave but with different intensity. Some problems in the incompressible prediction of P3 and P4 can be observed on the lower side denoting a different evaluation of the sectional effective angle of attack. The evaluation of the pressure coefficient on the retreating blade side, psi = 270°, shows a general better experimental-numerical correlation with only a leading edge under-expansion observed in P3 incompressible and P5 computations.

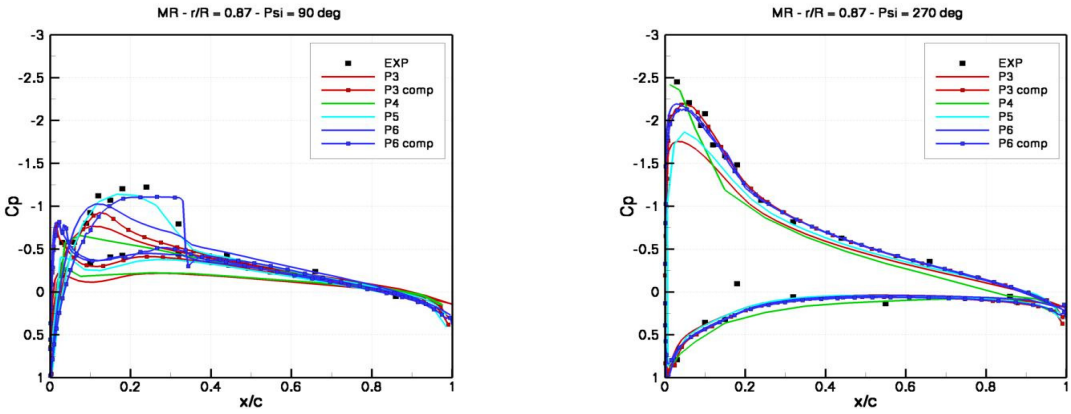

Figure 9: ID02 MR chordwise pressure coefficient

Figure 10 shows the pressure coefficients on the TR radial section r/R = 0.80 at different azimuthal steps for three test conditions. The experimental-numerical agreement in the ID02 is in general satisfactory. Some minor problems in the sectional effective angle of attack can be observed in some predictions at psi = 90° whereas at the azimuthal step psi = 270° P5 and P4 computations predict a lower expansion on the upper side respectively on the leading edge and over the whole chordwise extension. The analysis of the descent flight, ID05 indicates a very smooth behaviour of the pressure distribution, that was also observed in all the other azimuthal sections, and at both radial sections where the experimental results are available. The predictions provide a qualitative satisfactory agreement with the experiment with some discrepancies mainly on the airfoil lower side. Finally, the results of the ID13.1 test case show an example of varying agreements between the P5 and P6 predictions with the experiments: at psi = 90° P6 shows the best correlation with the experiment; at psi = 315° it is the P5 prediction that better correlates with the experiment.

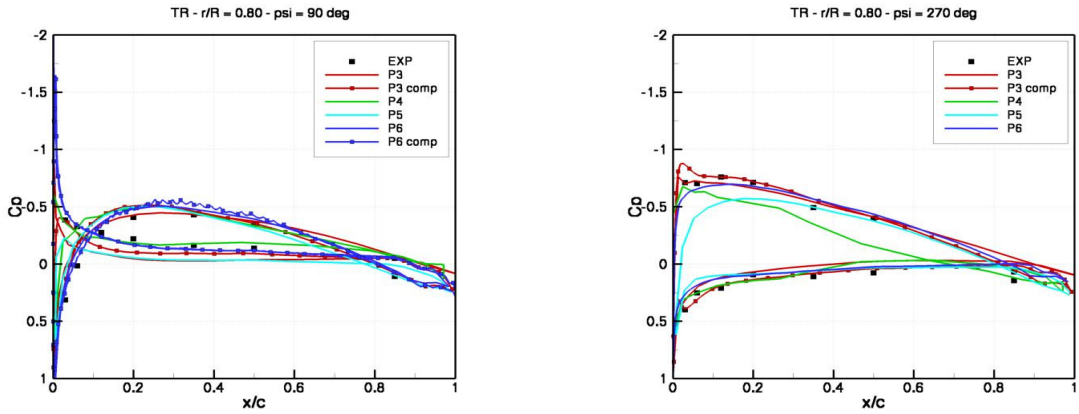

ID02

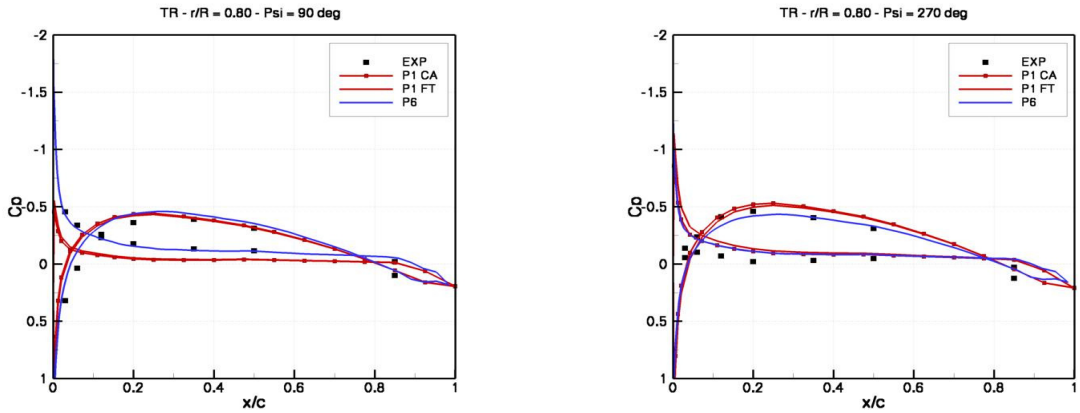

ID05

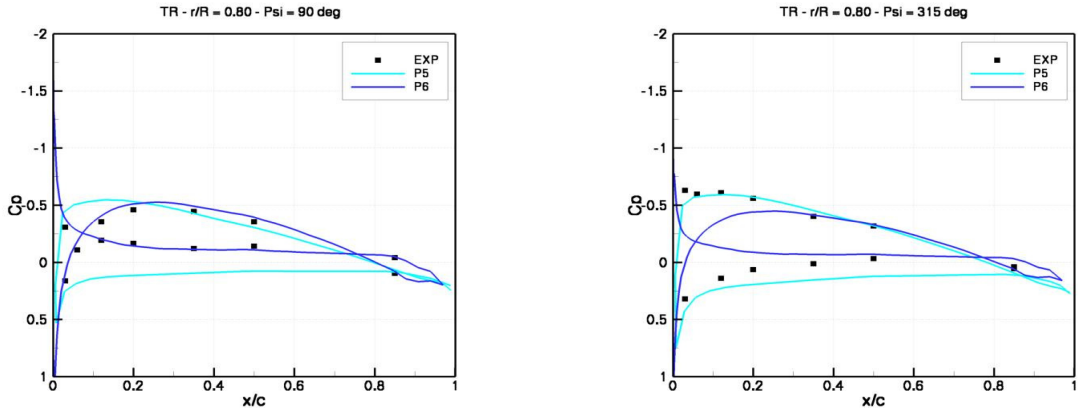

ID13.1

Figure 10: TR chordwise pressure coefficients at radial station r/R = 0.80

5.5 PIV analysis of TR region

A further validation of the aerodynamic prediction codes has been performed by the evaluation and comparison with the experimental PIV measurements of the three components of the velocities induced on two planes respectively located one in front of and the other behind the TR disc, [8]. Both aerodynamic data and PIV measurements have been shifted so that the centre of the tail rotor is the origin of the local axis. Moreover, the aerodynamic data have been handled so as to generate the component of the vorticity in the direction normal to the reference planes (out-of-plane vorticity). All the data shown in the pictures are vorticity contours plots ranging from -500 s^{-1} to +500 s^{-1}. Figure 11 illustrates the out-of-plane vorticity on Plane 1, located between the tail fin and the TR disc. The PIV data show considerable turbulence generated at the hub by the TR mast. In addition, the wake of the fin and the reflection of the laser light by the fin itself make the comparison with the numerical simulations somewhat difficult in the right part of the plots. The traces of the MR tip vortices can be detected as red nuclei of vorticity. Their position during the downstream convection can be clearly identified in the numerical simulation. The exact location is estimated at roughly the same position in all the simulations. A direct comparison with the experiment is possible only at psi=30° where the MR tip vortex can be easily detected just in front of the tail fin. In the other time instants the above indicated difficulties do not allow a correlation. Nuclei of different intensity and colour can be finally observed in all the simulations which are further traces of the complex wake system predicted in the TR disc region.

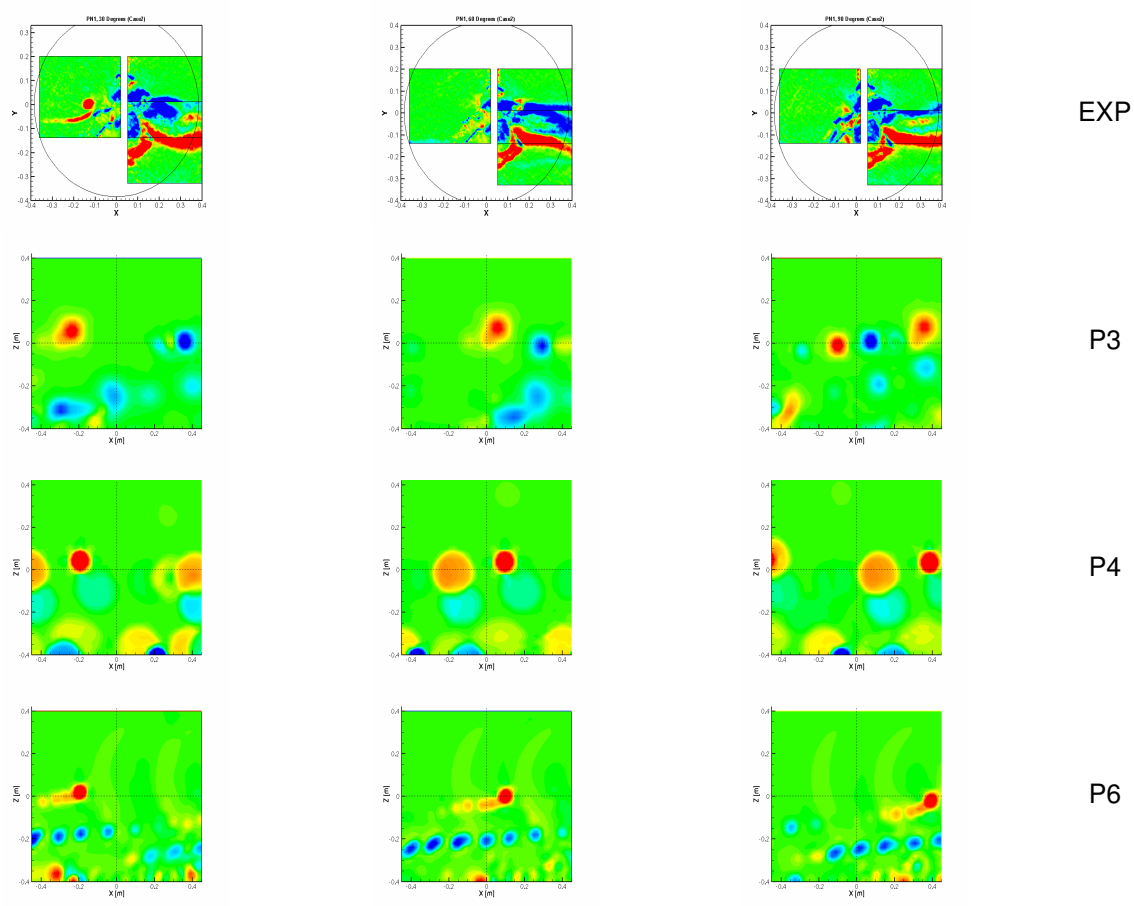

Figure 11: ID02 - PIV Plane 1 – Out-of-plane vorticity contours

Figure 12 illustrates the out-of-plane vorticity on Plane 2, located in front of the TR disc and immersed in the TR wake system. Since this plane does not intersect the TR mast and is sufficiently away of the tail fin, there is much less turbulence present and the traces of the MR tip vortices can be more easily detected. Both the PIV measurements and numerical prediction of these vortices do not differ much from those observed in Plane 1 thus indicating that the MR tip vortices may not be distorted by the orthogonal impingement with the TR blades. Clear indications of TR tip vortices traces can be now observed especially in the numerical simulations of P4 and P6.

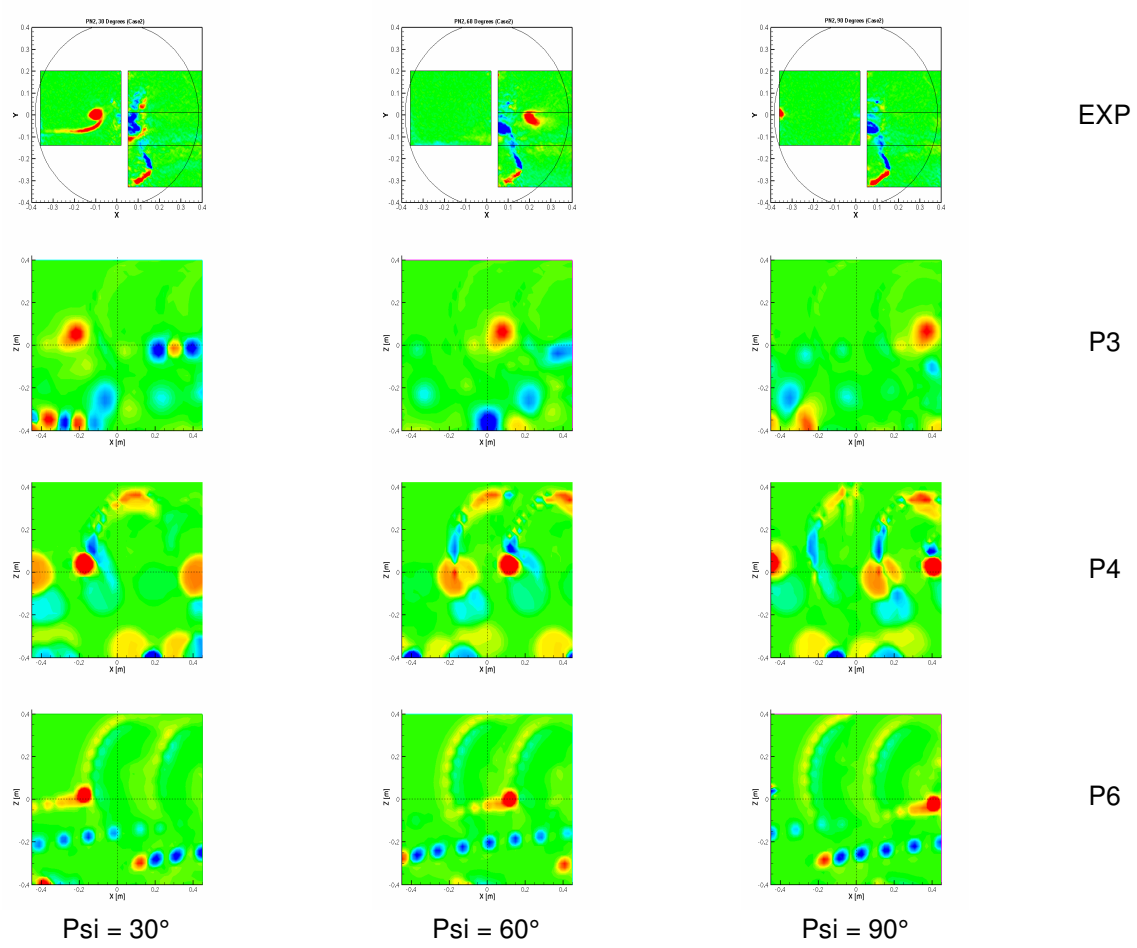

Figure 12: ID02 - PIV Plane 2 – Out-of-plane vorticity contours

6 CONCLUSIONS

The present paper presented a summary of the results obtained during the validation phase of the aerodynamic computational tools performed in the framework of the European research project HeliNOVI and relative to the interactional phenomena arising on a full helicopter configuration. The activity was carried out by performing seven test cases. Three baseline test cases were aimed at highlighting the phenomenological differences among the three main flight conditions that characterize the helicopter during a mission. The remaining four were dedicated to the analysis of possible TR modifications in order to alleviate those interactional aspects responsible for high TR noise emissions.

Three research centres: CIRA (I), DLR (D), and QinetiQ (UK); the EUROCOPTER industry; and the NTUA university (GR) participated in this activity.

The analysis of the experimental results highlighted the following main aspects:

1. for the baseline test cases the MR was trimmed at approximately the same thrust corresponding to a CT about equal to 5 x 10^{-3}. Therefore, the differences in CN were basically phenomenological: for ID01, 12° climb, a low-frequency unsteadiness with small amplitude was observed; for ID02, level flight, the amplitude was higher than ID01 and two regions of rapid change in the slope were observed: around 90° and (especially) 270°; for ID05, 6° descent, a high-frequency unsteadiness, typical of BVI phenomena, were observed at both advancing and retreating blade sides but with a smaller amplitude;
2. the comparison between the baseline level flight test case ID02 with those deriving from it showed no substantial changes in the MR CN time evolution. The only exception was represented by ID10 which was characterized by a lower tip speed of the two rotors;
3. the TR CT for the baseline test cases were different: the highest value was obtained for ID01 and the lowest for ID05. The resulting CN time history on the TR therefore showed a decided unsteady phenomenology with a consistent amplitude for the level flight condition and, conversely, a weaker unsteadiness and amplitude for the descent flight. These results could imply a smaller contribution of the TR to the global helicopter noise during the descent flight;
4. the comparison between the baseline level flight test case ID02, with those deriving from it indicated that the different changes in the TR operational characteristics had a common effect to reduce the frequency content of the TR CN unsteadiness without altering the amplitude of the time evolution with the only exception of ID10.

The comparison between the experimental results and the numerical ones highlighted once more the extreme complexity of the aerodynamic phenomena involved in a complete helicopter configuration operating at different flight conditions. This reflected on both measurements and simulations. In addition, in certain occasions there were indications that the available input information on the dynamics of the two rotor systems did not correspond to that of the model, which made the comparison even more difficult especially because of limited pressure data.

General conclusions through the numerical/experimental comparison for only one MR airfoil section or two TR airfoil sections could hardly been drawn. Nevertheless, the following main aspects were observed on certain occasions:

1. the applied methodologies were characterized by several differences in terms of: compressibility phenomena evaluation; fuselage modelling; blade deformation modelling and trimming procedures. It was common opinion that the different results obtained in terms of CN time history, mainly on the MR, were due more to the summation of these differences rather than to a specific one;
2. the effect of the elastic deformation modelling was, however, likely to play a special role in improving the quality of the numerical/experimental correlation. Indeed, it was observed that on the TR, where these effects played a secondary role, a better agreement was obtained;
3. the numerical/experimental comparison of the MR chordwise Cp pressure distributions showed a clear improvement in almost all the results when the compressibility was taken into account;
4. the interactional phenomena made the agreement among the various methodologies applied more difficult. This turned out to be particularly true for the TR which is directly involved in phenomena like blade/vortices impingement for which a finer time discretiza-

tion is necessary. The quality of the comparisons of the TR chordwise and time history Cp pressure distributions were of different degree: poorer for the climb flight, better for the descent flight;

5. the experimental results obtained for the ID13.X set of test cases showed a TR phenomenological complexity certainly lower than that of the corresponding baseline ID02 test case. This outcome provided a good indication about a possible implementation of one of these means for an effective TR noise reduction:
6. the comparison of the simulation with the PIV measurements showed a reasonable correlation of the MR tip vortices location and intensity thus indicating the ability of the predictions to correctly model the main characteristics of the complex wake system.

7 ACKNOWLEDGMENTS

The HeliNOVI project was partly supported by the European Union under the Competitive and Sustainable Growth Programme in the 5th Framework, Contract Nr. G4RD-CT-2001-40113.

8 REFERENCES

[1]. DLR, *"HeliNOVI – Annex I: Description of Work",* September 2001.
[2]. A. Visingardi, *"Final Validation Report of the Aerodynamic Prediction Codes",* HeliNOVI deliverable D1.4-2, March 2006.
[3]. H.-J. Langer, O. Dieterich, S. Oerlemans, O. Schneider, B. Van der Wall, J. Yin, *"The EU HeliNOVI Project - Wind Tunnel Investigations for Noise and Vibration Reduction",* 31st European Rotorcraft Forum, Florence, Italy, September 13-15, 2005.
[4]. J. Yin, B. Van der Wall, S. Oerlemans: *"Representative Test results from HELINOVI Aeroacoustic Main Rotor/Tail Rotor/Fuselage Test in DNW",* 31st European Rotorcraft Forum, Florence, Italy, September 2005.
[5]. J. Yin, *"HELINOVI Aeroacoustic Main/Tail Rotor Test in DNW: Test Documentation and Representative Results",* HeliNOVI deliverable D1.3-1, 06, February, 2006.
[6]. O., Dieterich, *"Wind Tunnel Model Database",* HeliNOVI deliverable D2.1-1, September 2002.
[7]. M. Stephan, V. Klöppel, H.-J. Langer, *"A new wind tunnel test rig for helicopter testing",* 14th European Rotorcraft Forum, September 1988.
[8]. A. Filippone, *"Validation of Post Test Aerodynamic Calculations with DNW PIV Data",* HeliNOVI deliverable D1.4-1, March 2006.